On the Formation of Whitecaps by a Threshold Mechanism. Part II: Monte Carlo Experiments

R. M. KENNEDY AND R. L. SNYDER

Nova University, Dania, FL 33004

(Manuscript received 10 April 1980, in final form 20 April 1983)

ABSTRACT

This paper is the second of three which seek to evaluate the hypothesis that deep water whitecapping is predictable in terms of a threshold mechanism involving the vertical acceleration.

The geometro-statistical computations of Part I of the series proceeded via direct integration of the joint probability densities for the vertical acceleration. In Part II we explore a second technique for computing whitecap statistics. This technique involves the Monte Carlo simulation of the vertical acceleration field and of the corresponding "breaking" variable field. Subsequent collation of various whitecap statistics parallels the analysis of whitecap photographs to be described in Part III.

Linear simulations for two types of JONSWAP spectra (Trials 1 and 2) and for a Pierson-Moskowitz spectrum (Trial 3) are presented. The resulting statistics, generated with limited resources, are sparse but pertinent. Significant improvement in the reliability of these statistics could be effected by using a vector processing computer.

1. Introduction

In Part I of this series we introduced the concept of a "breaking" variable. This variable assumes the values one or zero depending on whether or not breaking is present on the water surface at a specified space-time location, that is, on whether or not the corresponding downward acceleration exceeds a critical value. The breaking variable is a random field variable which contains a complete description of the surface geometry and surface geometrical statistics of the whitecapping process.

The statistics of the downward acceleration are described (to the linear approximation) by a joint Gaussian probability density function determined by the directional wave spectrum. Accordingly, the breaking variable statistics are expressible as integrals of this jointly Gaussian probability density function in which a threshold value is a limit of the integral. As discussed in Part I, however, the evaluation of these multi-dimensional integrals is neither analytically nor numerically trivial.

Examination of the statistics of interest, in particular, the geometrical moment statistics defined in Part I, suggests that in most cases it is numerically simpler to estimate these statistics from experimental data than it is to evaluate them analytically. It is in just such a case that the "method of statistical trials" [i.e., the Monte Carlo approach (Shreider, 1966)] becomes useful.

In the present case, this method generates (by analytical simulation) ensemble members of a stochastic process with the same statistical properties as the vertical acceleration field. Each ensemble member is searched for regions in space and time in which the critical value is exceeded. In those regions a binary breaking variable is set to one, indicating the presence of a whitecap.

Section 2 describes the linear field simulation method used and briefly describes a method for incorporating nonlinear effects into the simulation. Section 3 presents a set of statistics describing the deep water whitecap obtained from the Monte Carlo type simulations. Section 4 presents the results and Section 5 summarizes the resulting conclusions.

2. Simulation of wave fields

The Monte Carlo approach has found extensive use in the evaluation of complex engineering and physical problems. Methods of generating time series with preassigned statistics have been discussed in both physical and engineering literature. [For example, see Shreider (1966); Thompson (1973); Borgman (1969); and Eby (1970), as well as the reference lists of these works.]

In the present case it is necessary to synthesize the threshold field variable by generating time series at specific spatial locations. Two methods were implemented, both similar to that proposed by Borgman (1969). One of the methods closely parallels the paper by Eby (1970). This approach yielded satisfactory variables for the linear field cases but did not readily accommodate the addition of nonlinear effects. To

© 1983 American Meteorological Society

allow for this addition, a second method was implemented. We discuss the latter method only.

The synthesis of the vertical acceleration field is based on analytical models of that field variable. Our success in generating a field, largely indistinguishable from data, was possible because of the advanced state of the modeling of surface gravity waves. Because of the weak nonlinearities of the gravity wave field, we anticipate that linear analysis alone should yield a high-quality description of the actual ocean surface.

Following Hasselmann (1961), we represent the first-order surface elevation in the form

$$\zeta_1(\mathbf{x}, t) = \sum_{\mathbf{k}} \{Z_1^+(\mathbf{k}) \exp[i(\mathbf{k}\cdot\mathbf{x} - \omega t)] + Z_1^-(\mathbf{k}) \exp[i(\mathbf{k}\cdot\mathbf{x} + \omega t)]\}. \quad (1)$$

The complex Fourier amplitudes are independent Gaussian random variables satisfying the orthogonality conditions:

$$\langle Z_1^{\pm}(\mathbf{k})^* Z_1^{\pm}(\mathbf{k}')\rangle = \tfrac{1}{2}\Delta k_1 \Delta k_2 F_{\zeta^2}(\mathbf{k})\delta_{\mathbf{k}\mathbf{k}'},$$
$$\langle Z_1^{\pm}(\mathbf{k}) Z_1^{\pm}(\mathbf{k}')\rangle = 0,$$
$$\langle Z_1^{\pm}(\mathbf{k}) Z_1^{\mp}(\mathbf{k}')\rangle = 0,$$

where $F_{\zeta^2}(\mathbf{k})$ is the spectral density function (directional wave spectrum) and $\delta_{\mathbf{k}\mathbf{k}'}$ is the Kronecker delta function. Also because ζ_1 is real, we have

$$Z_1^{\pm}(\mathbf{k})^* = Z_1^{\pm}(-\mathbf{k}).$$

We next consider the change of independent variables $\mathbf{k} \rightarrow (\omega, \theta)$ with $\omega^2 = gk$, and rewrite (1) in the form

$$\zeta_1(\mathbf{x}, t) = \sum_{\omega>0} \sum_{\theta} (Z_1^+(\omega, \theta) \times \exp\{i[\omega^2 g^{-1}(x_1 \cos\theta + x_2 \sin\theta) - \omega t]\} + Z_1^-(\omega, \theta) \exp\{i[\omega^2 g^{-1}(x_1 \cos\theta + x_2 \sin\theta) + \omega t]\}),$$

where $Z_1^{\pm}(\omega, \theta)$ are complex amplitudes related to $Z_1^{\pm}(\mathbf{k})$. We note that the outer sum is over positive ω only:

$$Z_1(\omega, \theta) \equiv \begin{cases} Z_1^+(\omega, \theta), & \omega > 0 \\ Z_1^-(-\omega, \theta) = Z_1^+(-\omega, \theta + \pi), & \omega < 0. \end{cases}$$

We may rewrite this representation in the simpler form

$$\zeta(\mathbf{x}, t) = \sum_{\omega} \sum_{\theta} Z_1(\omega, \theta) \times \exp\{i[\omega^2 g^{-1}(x_1 \cos\theta + x_2 \sin\theta) - \omega t]\}, \quad (2)$$

where the outer sum runs over both positive and negative ω. The real and imaginary parts of the complex amplitudes $Z_1(\omega, \theta)$ are independent Gaussian variables with the variance

$$\langle [\mathrm{Re}(Z_1)]^2\rangle = \langle [\mathrm{Im}(Z_1)]^2\rangle = \tfrac{1}{4}\Delta\omega\Delta\theta E_{\zeta^2}(\omega, \theta), \quad \omega > 0,$$

where

$$E_{\zeta^2}(\omega, \theta) \equiv 2\omega^3 g^{-2} F_{\zeta^2}(\mathbf{k}).$$

The synthesis procedure may now be summarized as follows:

1) Choose a directional spectrum evaluated at a discrete set of frequencies and angles.

2) Determine the real and imaginary parts of the Fourier coefficients by choosing from a set of random numbers having zero mean, independent Gaussian amplitude distribution and variance:

$$\tfrac{1}{4}\Delta\omega\Delta\theta E_{\zeta^2}(\omega, \theta).$$

3) Evaluate the surface elevation from the expression

$$\zeta_1(\mathbf{x}, t) = \sum_{m=0}^{M-1} e^{-i\omega_m t}\{\sum_{n=0}^{N-1} Z(\omega_m, \theta_n) \times \exp[i\omega_m^2 g^{-1}(x_1 \cos\theta_n + x_2 \sin\theta_n)]\}.$$

The term in the braces is evaluated numerically for each ω_m. The surface elevation is then determined by a Fast Fourier Transform (FFT) at x for the times t_p, where

$$\left.\begin{aligned} t_p &= p\Delta t, \quad p = 0, 1, \ldots, M-1 \\ \Delta t &= \frac{2\pi}{M\Delta\omega} \end{aligned}\right\}.$$

In addition, the FFT requires that

$$Z_1(\omega_m, \theta_n) = Z_1^*(\omega_{M-m}, \theta_n).$$

4) Evaluate the vertical acceleration by letting

$$\Lambda_1(\omega, \theta) \equiv -\omega_m^2 Z_1(\omega_m, \theta_n),$$

and evaluating

$$\lambda_1(\mathbf{x}, t) = \sum_{m=0}^{M-1} e^{-i\omega_m t}\{\sum_{n=0}^{N-1} \Lambda_1(\omega_m, \theta_n) \times \exp[i\omega_m^2 g^{-1}(x_1 \cos\theta_n + x_2 \sin\theta_n)]\}.$$

A basic approach to synthesizing higher order nonresonant fields is to construct higher order nonresonant corrections to the linear field synthesized above. This may be accomplished directly from Hasselmann (1961), or equivalently by expressing the total field variable as a function power series of the first-order field. [Details of this latter procedure are given by Kennedy (1978).] While the resulting second-order correction appears straightforward, it would clearly be several orders of magnitude more time consuming

to evaluate than the linear expression. Accordingly, a second-order simulation was not attempted.

The space-time samples of the field variables are drawn from a stochastic process having a given directional spectrum. To the linear approximation, this spectrum is completely specified by the covariance matrix of the surface elevation. Thus, we may use a cross-spectral density matrix estimated from samples of the simulated surface elevation to verify the simulation itself (by comparing the estimated values with the theoretical matrix derived from the assumed directional spectra). Using this method, the quality of the simulations was closely checked and found to be high (Kennedy, 1978).

3. Monte Carlo experiment design

The experimental plan requires specification of three sets of items: independent variables, experimental parameters, and experimental statistics of interest. In the present case, the independent variables are time (t), and two space dimensions, downwind (x_1) and crosswind (x_2). Both sample intervals and the total field of view must be specified for each variable.

Similarly, there are three experimental parameters to be considered: the directional spectrum, the vertical acceleration critical value, and the highest frequency to be considered.

The experimental outcomes are the statistics of the breaking variable; i.e., statistics discussed in Part I. A principle objective of the experiment is to determine changes in breaking variable statistics caused by a change in an experimental parameter. This emphasis contrasts with attempting to determine precise statistics (which would require considerably more data.)

A principal limitation to the numerical experiment was the cost of simulating the field variables. As will be shown in this section, the required number of space-time data points is quite large. For example, a typical "trial" required over two million data points, and the total experiment had three trials. Simulation costs severely restricted experimental objectives; thus, ultimate experiment design was a compromise between objectives and cost.

The primary factor controlling the cost of a particular object is statistical accuracy. For example, while 25 whitecaps might be required to estimate the mean whitecap duration with a 20% error, 100 whitecaps would be required to obtain 10% errors.

Three types of directional spectra were employed. These are the JONSWAP spectrum (Hasselmann and others, 1973) chosen as representative of a fetch-limited sea (Trials 1 and 2) and the Pierson–Moskowitz spectrum (Pierson and Moskowitz, 1964), chosen as an example of a fully developed sea (Trial 3), and a third experimentally determined spectrum, from the field experiment, presented in Part III. Because of several problems with the third simulation, it will not be discussed in detail.

The first two spectra are defined as follows:

1) Pierson–Moskowitz spectrum[1]

$$D_{\zeta^2}(\omega) = 0.0081 g^2 \omega^{-5} \exp\left[-\frac{5}{4}\left(\frac{\omega}{\Omega}\right)^{-4}\right],$$

where

$$\Omega = 0.088\,\frac{g}{W}.$$

2) JONSWAP spectrum

$$D_{\zeta^2}(\omega) = \epsilon g^2 \omega^{-5} \exp\left[-\frac{5}{4}\left(\frac{\omega}{\Omega}\right)^{-4}\right] \gamma^{\exp\left[-\frac{(\omega-\Omega)^2}{2\sigma^2\Omega^2}\right]},$$

where $\tilde{\Omega} = 22\tilde{x}^{-0.33}$, $\gamma = 3.3$, $\sigma = 0.08$, $\tilde{\Omega} = \Omega W/g$, $\epsilon = 0.57\tilde{x}^{-0.5}$, and $\tilde{x}$ is a nondimensional fetch.

In both theoretical spectra $E_{\zeta^2}(\omega, \theta)$ was taken to be of the form

$$E_{\zeta^2}(\omega, \theta) = D_{\zeta^2}(\omega) H(\theta).$$

The spreading function significantly influences the geometrical shape of the whitecap. A frequency-independent form which does not allow any waves traveling against the wind was employed. The form is

$$H(\theta) = \begin{cases} A \cos^r\theta, & -\dfrac{\pi}{2} \leqslant \theta \leqslant \dfrac{\pi}{2} \\ 0, & \text{elsewhere.} \end{cases}$$

A is evaluated such that

$$\int_{-\pi}^{\pi} d\theta H(\theta) = 1.$$

Exponent values of 2 and 4 were used to study the effect of the spreading function on the statistics of the breaking variable.

The integral of the acceleration spectra is non-convergent. This makes it necessary to choose an upper cutoff frequency. The consequence of choosing such a frequency on whitecap shape is discussed below. (See also the discussion in Part I.)

The highest frequency of interest to this study is taken to be the spatial resolution of the observer. In the numerical experiments to be described, the "cam-

[1] A modified form of the Pierson-Moskowitz spectrum is employed so that Ω retains its identity as the frequency of peak energy. W is the wind speed.

era" height is always adjusted so that the field of view is a rectangle whose sides are approximately a half-wavelength of the principal wave component of the surface elevation field. Numerical experiments were carried out to determine what the highest frequency should be relative to this point of view. Employing qualitative criteria, it was concluded that a highest frequency of three times the frequency of peak energy adequately described the larger whitecaps. Higher frequencies did not significantly alter the shape of the large breakers, but rather only added small-scale incipient whitecaps.

It should also be noted that there is a strong economic motivation to keep the highest frequency included as small as possible. The higher the cutoff frequency the more frequency bands involved in the superposition and (because of the correspondingly smaller spatial resolution) the more grid points needed in the simulation field.

Throughout the Monte Carlo experiments several critical values of acceleration were chosen. It is useful, however, to obtain a rough estimate of a critical value from field data. The BOMEX directional spectra of Regier and Davis (1977) were measured simultaneously with measurements of percentage whitecap coverage by Monahan (1971). The fraction of the surface covered by breaking water is directly calculable from the acceleration spectra and a critical value as shown in Part I. Thus, knowing the acceleration spectra and the percentage whitecap coverage allows one to calculate the critical value.

Comparison of the percentage whitecap coverage during the BOMEX experiment with the BOMEX acceleration values indicates that a single critical value will not match all of the data. This is because the whitecap data show an order of magnitude change in whitecap coverage over the wind speed range of 5–10 m s^{-1} (i.e., 0.2–2%) while the acceleration value changed only 11% over this same range. If one were to choose an independent critical value to best match the data at the wind speeds, one would obtain $0.52g$ at 5 m s^{-1}, $0.51g$ at 7.5 m s^{-1}, and $0.40g$ at 10 m s^{-1}. While these values are all of the order of $0.5g$, they appear to decrease with increasing wind speed. This decrease may reflect uncertainties in the BOMEX/Monahan data or it might be real, in which case a possible explanation for the change is that the surface drift current, which increases with wind speed, reduces that critical value by the mechanism discussed by Phillips and Banner (1974).

The experimental outcomes were quite sensitive to the choice of critical value and a "reasonable range" of values was quite evident. When the critical value chosen was too low, it manifested itself by a set of whitecaps which had shapes contrary to observations. On the other hand, if the chosen values were too high, the percentage of whitecap coverage rapidly became zero. It is quite satisfying that the range of "reasonable" values closely matched the values estimated from the BOMEX data. The experimental values used are 35%, 40%, 45% and 50% of the gravitational constant for Trials 1 and 2, and 25%, 30%, 35% and 40% for Trial 3.

A summary of the experimental conditions for each of the three trials implemented is given in Table 1.

In an effort to provide a direct comparison with the experimental statistics to be generated in Part III, the third and final Monte Carlo simulation was effected using the experimentally determined directional spectrum for runs 13, 14, 15 from December 1972 (see Fig. 3 of Part III). Two problems significantly degrade this comparison: 1) The experimentally determined directional spectrum extended only to twice the peak frequency which is a poor match with the corresponding cutoff frequency associated with the photographic threshold. 2) Because the observed whitecap coverage for the experimental runs

TABLE 1. Experimental parameter summary.

Trial No.	Directional spectra type	Non-dimensional fetch	Wind speed (m s^{-1})	Spreading function	Critical values	Frequency of peak energy (rad s^{-1})	Highest frequency (rad s^{-1})	Spatial sampling interval (m)
1	JONSWAP	10^3	10	$\cos^2\theta$, $\lvert\theta\rvert < \frac{\pi}{2}$ 0, elsewhere	$0.35g$ $0.40g$ $0.45g$ $0.50g$	2.21	6.75	0.2
2	JONSWAP	10^3	10	$\cos^4\theta$, $\lvert\theta\rvert < \frac{\pi}{2}$ 0, elsewhere	$0.35g$ $0.40g$ $0.45g$ $0.50g$	2.21	6.75	0.2
3	Pierson-Moskowitz	—	10	$\cos^2\theta$, $\lvert\theta\rvert < \frac{\pi}{2}$ 0, elsewhere	$0.25g$ $0.30g$ $0.35g$ $0.40g$	0.981	2.94	1.02

is typically an order of magnitude smaller than in the previous simulations, an order of magnitude increase in the length of the simulations is required for comparable statistical reliability. As such an increase was not practical we decided instead to attempt the simulation at a reduced threshold value ($0.15g$ and $0.2g$). The resulting whitecap statistics (which will not be presented) do not compare favorably with the results of the field experiments. (Although there is reasonable agreement between some of the moment statistics.) Because the sense of the discrepancies are typically in keeping with the lower cutoff frequency and the lower threshold levels for the simulation, we believe they are probably the result of these factors and do not represent a failure of the threshold model.

A principal difficulty with performing a whitecap experiment, either in the field or numerically, is the fleeting, random nature of the event. Accordingly, space–time observations require high resolution and a large field of view. A large space–time field of view is needed to acquire a reasonable number of events, while high resolution is required to adequately describe each event. These conflicting requirements necessitate accumulating a large number of samples.

In order to fix the resolution, a space–time correlation function of the breaking variable was computed. The space–time interval was chosen such that a space–time delay of one sample interval yielded a positive normalized correlation value of about 50%. A JONSWAP-type one-dimensional directional spectra with a $\cos^2\theta$ spreading function and typical critical values were used in this development. This computation suggested that a temporal sample interval should be $\sim 2\%$ of the period of the frequency of peak energy and the downwind spacial interval was also 2% of the wavelength of the frequency of peak energy. As anticipated from visual observations of whitecaps, this dimension was almost twice as large in the crosswind direction (3.5%). It would thus be possible to have different sampling intervals in the downwind and crosswind directions. However, because of the trial-to-trial variability of the correlation values and the desire to describe the spatial shapes as closely as possible, the downwind and crosswind sampling intervals were both set equal to 2% of the wavelength of the frequency of peak energy.

The two-dimensional spatial aperture was then chosen to be as large as computer size and costs would allow. The number of breaking variable "sensors" (i.e., spatial points) increases as the square of the aperture. A realistic number turned out to be a 24-by-24 element array, yielding 576 "sensors". The spatial aperture thus turned out to be just short of half a wavelength of the frequency of peak energy. The temporal length of an experimental run was about 10 periods of the frequency of peak energy.

A typical experimental run consisted of 512 time samples at each of the 576 "sensors." There were seven runs per trial, and three trials.

4. Results

In this section we present the statistical description of the breaking variable from the Monte Carlo simulations. The statistics estimated are either discussed at length in Part I or are self-explanatory. Each statistic is estimated for a set of critical values. The experimental parameters and critical value set are listed in Table 1.

Before proceeding with a detailed look at the results, special note should be made of the conditions of Trial 3 which used a Pierson-Moskowitz spectrum (evaluated for a 10 m s^{-1} wind speed and a cosine-squared spreading function). This change in spectrum type from the JONSWAP spectrum of Trials 1 and 2 significantly changes the surface elevation field; in particular, it reduces the mean-square vertical acceleration and therefore the whitecap coverage. This reduction is primarily a result of the decreased value of the Phillips equilibrium constant and of the peak enhancement factor (equal to 1) for the Pierson-Moskowitz spectrum. A consequence of this approach is the reduction in whitecap coverage for a given critical value. The occurrences of the larger whitecaps are infrequent, which reduces the efficiency of the simulation procedure. To increase the number of whitecaps in the trials to a reasonable number, the range of critical values was changed to $0.25g$–$0.40g$ for Trial 3. This did increase the number of whitecaps observed during the experiment but, since the breakers are occurring at a smaller critical value, the intra-trial comparisons must be made cautiously.

The most fundamental of the primary statistics is the percentage whitecap coverage or, equivalently, the probability of breaking. This statistic may be easily calculated analytically as shown in Part I (Fig. 5). The results of this calculation are compared with the data from all 21 runs of the numerical experiments in Fig. 1 as a function of λ_{rms}/Λ_c. An important point to be noted from this figure is the highly sensitive dependence of the whitecap coverage on a_{rms}.

The dependence of the probability of breaking on critical value is illustrated in Fig. 2, where trial averages are used. The directional spectrum type is also shown in Fig. 2 which illustrates that λ_{rms} (which successfully coalesces the data) is the only spectral parameter of importance.

As would be anticipated, the number of new whitecaps observed in a trial depends critically on the assumed threshold value. A 30% reduction in critical value increased the number of whitecaps by 517%. Since the number of whitecaps counted occurred over a specific space and time interval, the meaningful statistic is the number of whitecaps per unit area and time. These values are given in Table 2.

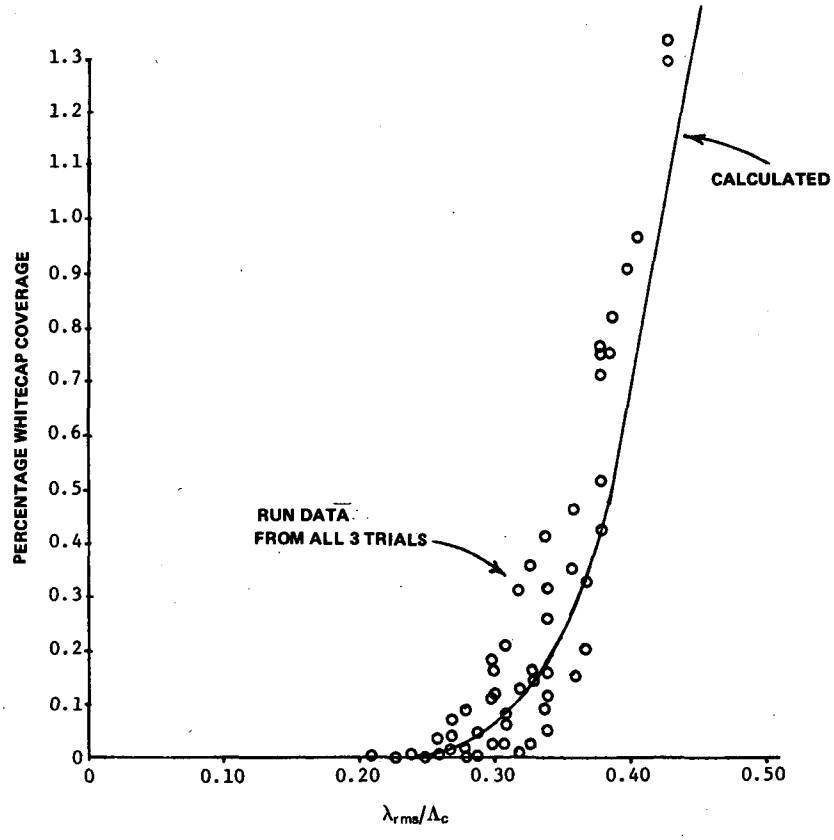

FIG. 1. Whitecap coverage versus rms acceleration.

A very useful and basic statistic estimated is the space–time correlation function of the breaking variable (see Part I for the explicit definition). Figs. 3 and 4 illustrate a typical normalized correlation function. The independent variables for Fig. 3 are downwind separation and time delay, while in Fig. 4 they are crosswind separation and time delay. The third dimension in both figures is the value of the normalized correlation function for various combinations of the two independent variables. Note that combination values of downwind and crosswind separation were not evaluated; that is, the spatial separation was never oblique to the wind.

Because of the expense of the correlation calculation, it was not repeated at each critical value. The correlation function was calculated at $0.4g$ for Trials 1 and 2, and $0.3g$ for Trial 3.

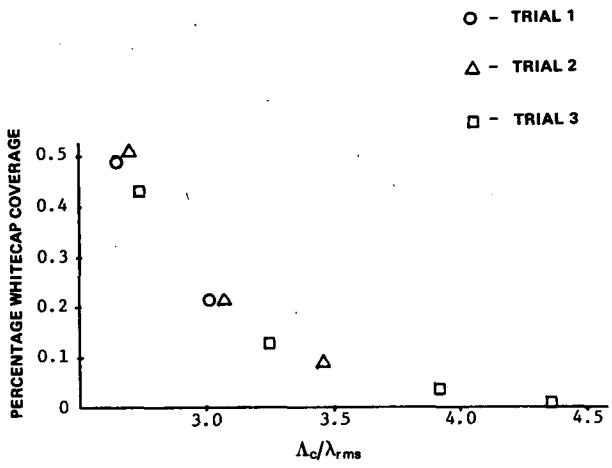

FIG. 2. Whitecap coverage vs. critical value.

TABLE 2. Summary of number of whitecaps per unit area per unit time.

Non-dimensional critical value Λ_c/g	Trial 1 JONSWAP $\tilde{x} = 10^3$ $\cos^2\theta$	Trial 2 JONSWAP $\tilde{x} = 10^3$ $\cos^4\theta$	Trial 3 Pierson-Moskowitz $\cos^2\theta$
0.25	—	—	0.00039
0.30	—	—	0.00013
0.35	0.020	0.015	0.00005
0.40	0.010	0.008	0.00001
0.45	0.004	0.004	—
0.50	0.003	0.003	—

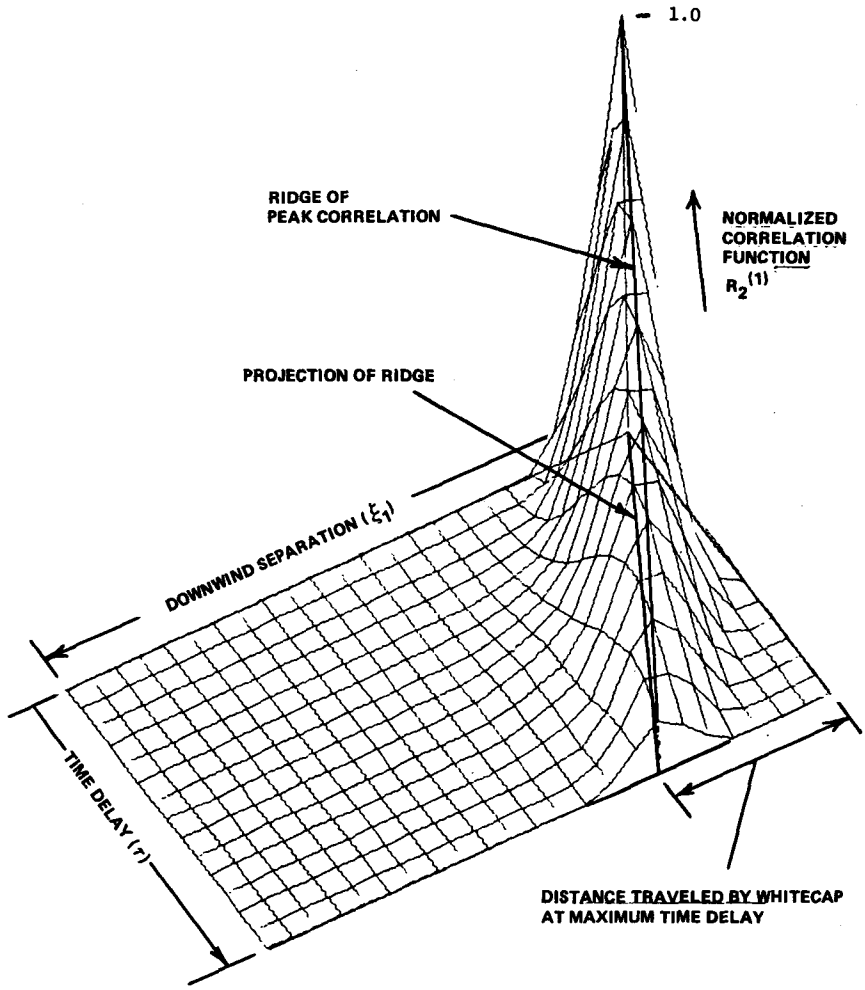

FIG. 3. Downwind-time correlation of breaking variable.

Various length and time scales were obtained from the correlation functions. Two types of correlation scales are given.

One is an integral scale defined as the integral of the normalized correlation function. The second type of scale is a 50% scale. This is defined as the space or time separation required for the correlation function to decline by 50% of its maximum value (which occurs at zero space and time separation). The trial average of the above length scales is determined by averaging the individual runs.

A breaking variable propagation velocity is also obtained by taking the slope of the "ridge" of the downwind–time correlation function. Fig. 3 illustrates this procedure. The essence of the process is that one determines the separation required to spatially keep up with the breakers' downwind movement. The ratio of this length to time defines the desired velocity.

Of primary interest is the dependence of the length and time scales and the whitecap propagation velocity on the choice of directional spectrum type. As will be shown, the wavelength and period of the component of the field having the frequency of peak energy of the spectrum is an important parameter. However, the spreading function clearly alters the crosswind-length scales. Thus a simple parameterization of this dependence is important. To develop a parameter, which expresses the length scale dependence on the spreading function, we proceed as follows:

Let the field $\zeta_1(\mathbf{x}, t)$ observed near the origin of the coordinate system ($\mathbf{x}$) be due to a superposition of plane waves having the same amplitudes and wavenumber. We consider two "sensors" placed symmetrically about the origin and oriented either downwind or crosswind. A correlation function between these two sensors may now be defined as

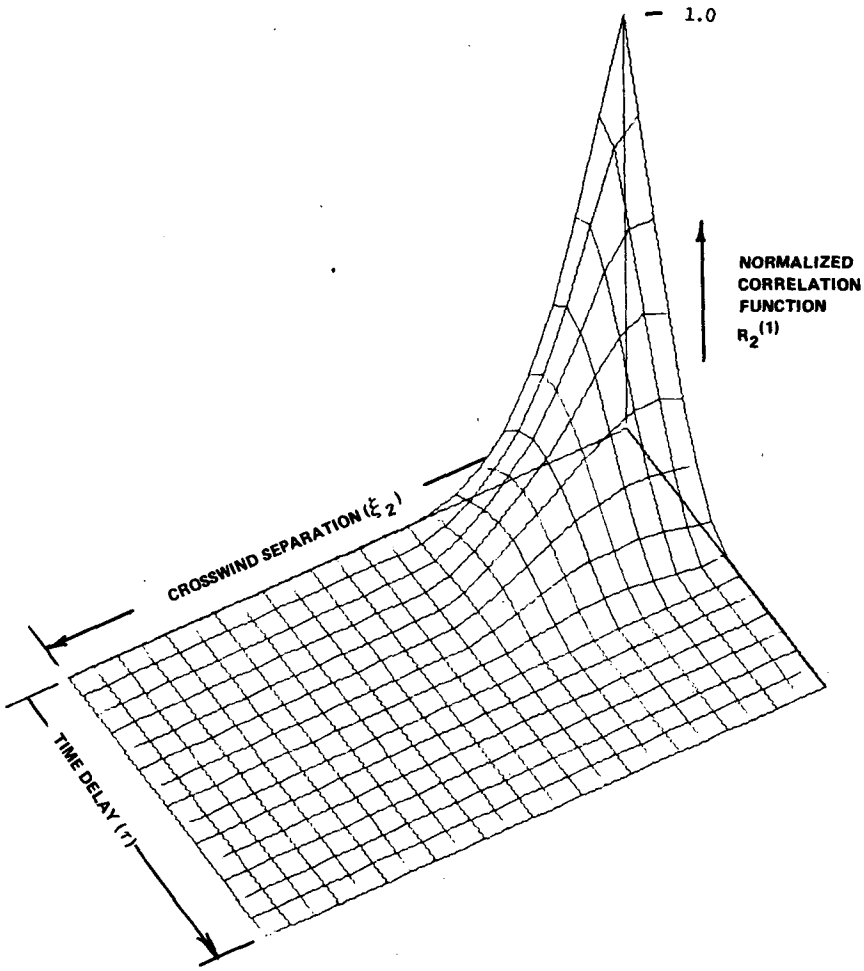

FIG. 4. Crosswind-time correlation of breaking variable.

$$C_{\zeta^2}(\xi, 0) = \langle \zeta(-\tfrac{1}{2}\xi, t)\zeta^*(\tfrac{1}{2}\xi, t)\rangle.$$

If the sensors are crosswind of one another we have

$$C_{\zeta^2} \sim \int_{-\theta_H}^{\theta_H} d\theta \exp(ik\xi_c \sin\theta),$$

where θ_H is the extent of the spreading function. Similarly if they are downwind of one another

$$C_{\zeta^2} \sim \int_{-\theta_H}^{\theta_H} d\theta \exp(ik\xi_d \cos\theta).$$

We now define the length scales associated with a spreading function width of θ_H. Specifically, these are the values required for the normalized correlation to be 50% of its maximum value; ξ_c satisfies the integral equation

$$\frac{2}{\theta_H}\int_0^{\theta_H} \cos(k\xi_c \sin\theta)d\theta = 1.$$

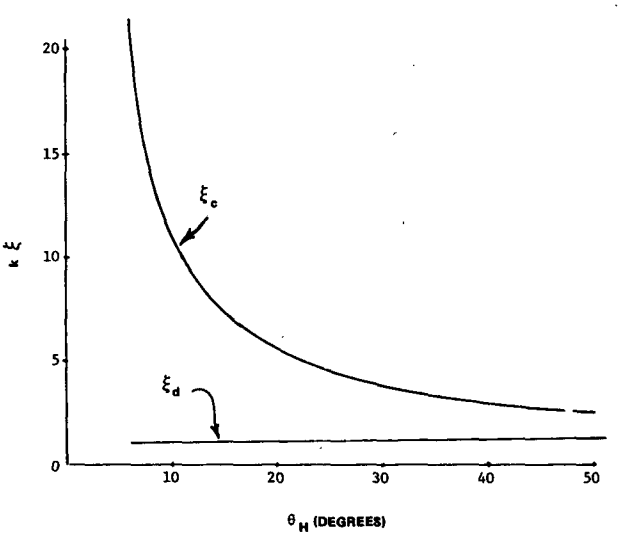

FIG. 5. Length scales parameterizing directional spectrum type.

TABLE 3. Length scale.

	Principal wavelength (m)	Spreading function dependent scale		Length scale		Nondimensional length scale		Nondimensional length scale	
		Downwind (m)	Crosswind (m)	Downwind (m)	Crosswind (m)	Downwind	Crosswind	Downwind	Crosswind
				a. Integral length scale.					
Trial 1	12.2	2.2	5.0	0.22	0.39	0.018	0.032	0.099	0.077
Trial 2	12.2	2.1	6.6	0.21	0.51	0.017	0.042	0.100	0.077
Trial 3	64.1	11.7	26.5	1.01	1.76	0.016	0.028	0.086	0.066
				b. Fifty percent correlation length scale.					
Trial 1	12.2	2.2	5.0	0.18	0.32	0.015	0.026	0.082	0.064
Trial 2	12.2	2.1	6.6	0.18	0.42	0.015	0.034	0.086	0.064
Trial 3	64.1	11.7	26.5	0.88	1.48	0.014	0.023	0.075	0.056

In a similar manner, the downwind length scale ξ_d satisfies the integral equation

$$\frac{2}{\theta_H}\int_0^{\theta_H} \cos(k\xi_d \cos\theta)d\theta = 1.$$

The latter equation is not single valued in ξ_d, and thus we will choose the smallest value. Fig. 5 summarizes the solutions to the above integral equation.

Table 3 summarizes both the integral length scales and the 50% correlation scales. Table 4 does the same for the time scales. Both tables clearly show that the space and time scales of a whitecap are completely determined by the space and time scales of the wave component having the frequency of peak energy and (in the case of the crosswind length scale) by the spreading function width (θ_H).

The whitecap propagation velocity is seen (Table 5) to be significantly smaller than the phase speed of the component of the field having the frequency of peak energy. The magnitude is close to the group velocity associated with the frequency of peak energy. This similarity is probably coincidental, as there appears to be no reason to believe that group velocity is a pertinent parameter. Most likely the velocity of the whitecap which coincides with the velocity of the negative peaks of the vertical acceleration field reflects the importance of the higher frequencies to the breaking process.

It is instructive to classify the statistics into two groups. This type of classification is an advantage because of the two different types of data analysis encountered. In some cases, the statistics of interest may be determined from the value of the breaking variable in a fixed space–time coordinate system. Such statistics will be referred to as "breaking variable statistics" of which the above statistics are examples. Other statistics, which describe characteristics of the evolution of a whitecap, are most efficiently estimated by "collecting" many whitecaps occurring at various times and places, and subsequently moving them to a relative coordinate system in which they are aligned such that the initial breaking point occurs at the origin. Thus each whitecap becomes an ensemble member of the same stochastic process. Such statistics will be referred to as "event statistics."

It has been mentioned several times throughout the text that the length and number of simulations was limited by the expense of the process. This limit has been felt most severely in the area of event sta-

TABLE 4. Time scale.

	Principal period (s)	Fixed coordinate time scale (s)	Nondimensional fixed coordinate time scale	Moving coordinate time scale (s)	Nondimensional moving coordinate time scale
			a. Integral time scale summary.		
Trial 1	2.79	0.096	0.034	0.267	0.096
Trial 2	2.79	0.104	0.037	0.276	0.099
Trial 3	6.41	0.204	0.032	0.631	0.098
			b. Fifty percent correlation time scale summary.		
Trial 1	2.79	0.085	0.030	0.232	0.083
Trial 2	2.79	0.089	0.032	0.276	0.099
Trial 3	6.41	0.180	0.028	0.771	0.120

TABLE 5. Whitecap propagation velocity summary.

	Phase velocity of principal component (m s^{-1})	Whitecap velocity (m s^{-1})	Nondimensional whitecap velocity
Trial 1	4.36	2.27	0.52
Trial 2	4.36	1.90	0.44
Trial 3	10.01	4.25	0.43

tistics, since only whitecaps which are complete in the space–time field of view of the simulation can be used in the estimations. The number of complete events per trial is in some cases quite small, and the corresponding statistical error large, which can obscure small intra-trial differences.

In general all event statistics displayed an insensitivity to the critical value. In no case was a critical value dependence reliably observed over the range of critical values employed. While small differences must surely exist, the lack of data (degrees of freedom) at the higher critical values prevented our observing them. The physical insight to be gained here is that higher peaks rise rapidly through the range of critical values, making the statistic relatively insensitive to the critical value.

The simplest of the event statistics is the average zero-order space–time moment ($\langle M_{000} \rangle$) which measures the space–time extent of the whitecaps. Table 6 illustrates the collapsing of these data by nondimensionalizing by the scales of the frequency of peak energy.

The second statistic of interest is the instantaneous area covered by a whitecap. It is described by the moment M_{00}. Examples of this area, as a function of time, are shown in Fig. 6. Fig. 7 shows the ensemble average dependence, where the average was taken over all whitecaps for a particular trial at a given critical value. Only those critical values having more than 10 whitecaps are shown. Nondimensionalization by k_0 and Ω clearly coalesces the data.

A statistic related to the time-dependent whitecap area is the average whitecap temporal duration. The large difference of values between Trials 1 and 2 with Trial 3 is readily reduced by scaling by Ω. This statistic is shown in Table 7.

TABLE 6. Nondimensional zero-order space-time moment (Table entries are $k_0^2 \Omega M_{000}$).

	Critical value Λ_c/g					
	0.25	0.30	0.35	0.40	0.45	0.50
Trial 1	—	—	0.166	0.129	0.203	0.096
Trial 2	—	—	0.209	0.230	0.230	0.268
Trial 3	0.153	0.136	0.098	0.028	—	—

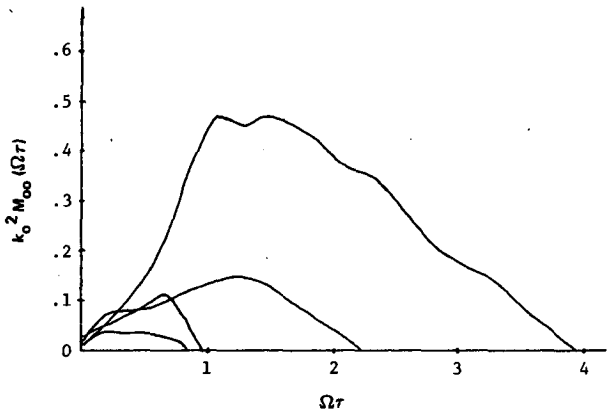

FIG. 6. Examples of total whitecap area as a function of time. Trial 1—critical value: 0.4g.

Total swept area is a physically important quantity, since it measures the amount of water surface "churned up" by the whitecap. This statistic is shown in Table 8.

A measure of the propagation velocity of the whitecap is obtained by determining the velocity of the

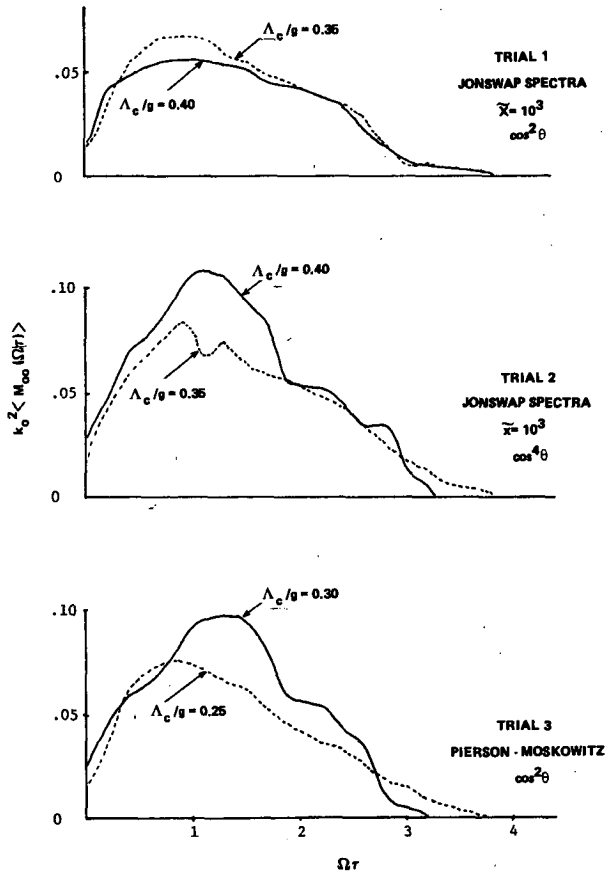

FIG. 7. Average total area as a function of time.

TABLE 7. Nondimensional whitecap duration (Table entries are ΩT).

	Critical value Λ_c/g					
	0.25	0.30	0.35	0.40	0.45	0.50
Trial 1	—	—	1.50	1.43	1.61	1.65
Trial 2	—	—	1.67	1.76	1.98	2.20
Trial 3	1.53	1.69	1.56	0.98	—	—

center of mass of the whitecap. Typical values of the downwind and crosswind center of masses are shown as a function of nondimensional time in Fig. 8. The downwind movement is seen to be as constant as the crosswind movement is variable. A velocity was defined as the difference between the final and initial position divided by the whitecap duration. Scaling the mean values by the phase speed of the spectral component having the frequency of peak energy indicated that the average downwind velocities of the three trials were 46, 44 and 45% of the respective phase speeds. This is consistent with the results found from the breaking variable correlation function.

The second central moments, M_{10} and M_{01}, describe the downwind and crosswind extent of a whitecap. Examples of typical time dependence are shown in Fig. 9. The time average of the quantities can be found for each whitecap; then the ensemble average of this time average yields an overall average. Scaling the mean values of this statistic by k_0 does a reasonable job of coalescing the data, as shown in Table 9. Although the scatter is large, comparison of Trial 1 and 2 results shows the difference between the $\cos^2\theta$ and $\cos^4\theta$ spreading functions. The data were then nondimensionalized by a factor reflecting the different spreading factor (see Fig. 5). The result of this scaling is shown in Table 10. Here we see good collapse of both downwind and crosswind data.

5. Conclusions

A summary of the principal results of the experiments is as follows:

1) The percentage whitecap coverage (or, equivalently, the probability of breaking) is a highly sensitive function of the root-mean-square acceleration level.

2) The propagation velocity of the whitecap was typically 0.45% of the phase velocity associated with the frequency of peak energy. While this velocity is

TABLE 8. Nondimensional total swept area (Table entries are $k_0^2\langle A_s\rangle$).

	Critical value Λ_c/g					
	0.25	0.30	0.35	0.40	0.45	0.50
Trial 1	—	—	0.433	0.270	0.370	0.277
Trial 2	—	—	0.363	0.424	0.504	0.489
Trial 3	0.307	0.428	0.255	0.101	—	—

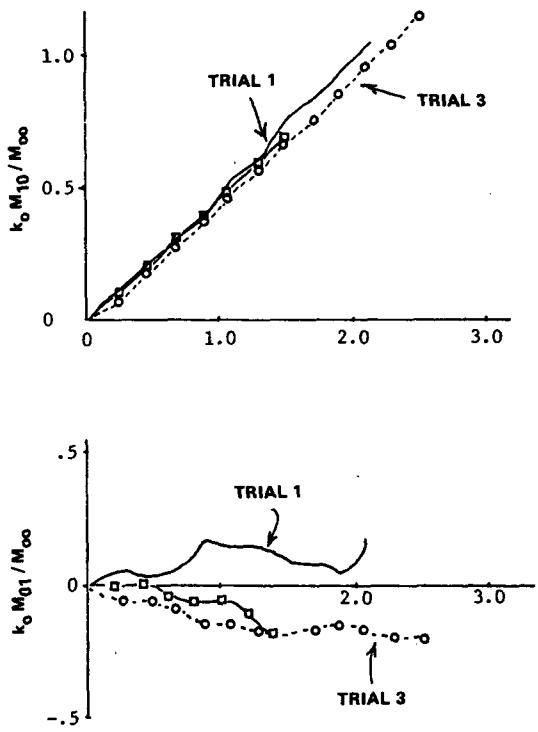

FIG. 8. Examples of center of mass time dependence.

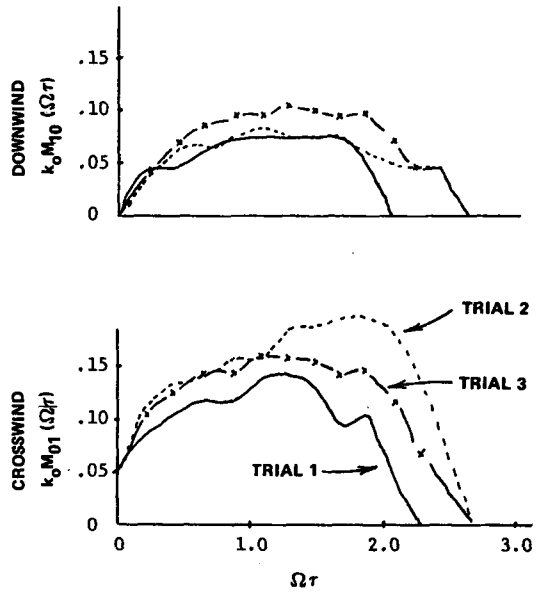

FIG. 9. Examples of second central moments as a function of time.

TABLE 9. Second central moment scaled by k_0.

	Critical value Λ_c/g					
	0.25	0.30	0.35	0.40	0.45	0.50
a. Nondimensional downwind second central moment (Table entries are $k_0\langle\bar{M}_{10}\rangle$.)						
Trial 1	—	—	0.035	0.035	0.025	0.010
Trial 2	—	—	0.025	0.035	0.044	0.049
Trial 3	0.032	0.045	0.034	0.016	—	—
b. Nondimensional crosswind second central moment (Table entries are $k_0\langle\bar{M}_{01}\rangle$.)						
Trial 1	—	—	0.069	0.069	0.084	0.069
Trial 2	—	—	0.079	0.099	0.113	0.118
Trial 3	0.098	0.092	0.074	0.032	—	—

close to the group velocity, the similarity between the two velocities is probably coincidental, as there appears to be no reason to believe that group velocity is a pertinent parameter. The low velocity of the whitecaps probably reflects the importance of the higher frequency wave components to the breaking process.

3) The amplitude distribution of the event statistics shows no statistically significant differences over the range of critical values. This is a consequence of two factors: first, the statistic appears to be relatively insensitive to the critical value as opposed to the highly sensitive nature of the percent whitecap coverage, and, second, the lack of data (degrees of freedom) at the higher critical values does not allow the statistical resolution necessary to observe the differences which surely must exist. The physical insight to be gained here is that higher peaks rise rapidly through the range of critical values making the duration relatively insensitive to the critical value.

TABLE 10. Second central moment scaled by k_d.

	Critical value Λ_c/g					
	0.25	0.30	0.35	0.40	0.45	0.50
a. Downwind second central moment (Table entries are $k_d\langle\bar{M}_{10}\rangle$.)						
Trial 1	—	—	0.18	0.18	0.13	0.05
Trial 2	—	—	0.14	0.20	0.25	0.28
Trial 3	0.17	0.24	0.18	0.08	—	—
b. Crosswind second central moment (Table entries are $k_c\langle\bar{M}_{01}\rangle$.)						
Trial 1	—	—	0.17	0.17	0.20	0.17
Trial 2	—	—	0.14	0.18	0.20	0.21
Trial 3	0.18	0.22	0.18	0.08	—	—

4) The directional spectrum dependence of all event statistics is dominated by the space and time scales of the spectral component having the frequency of peak energy. The crosswind extent of the whitecaps, however, also depends on the effective angular width of the spreading function. This same conclusion applies to the space–time scales of the breaking variable correlation function.

Several inadequacies of the model should be pointed out. While it is difficult to quantitatively assess the seriousness of these omissions, they are noted as follows:

- There is no feedback between the breaker and the wave field which would allow a whitecap to modify the form of the wave field.
- It was not possible for the critical value to be locally changed; that is, conditions of the acceleration field could not modify the critical value.
- While a method of incorporating nonlinear effects into the calculations was developed, it was not used.
- A depth-dependent drift current was not included.
- Computation of whitecap statistics via Monte Carlo simulation of the wave field is practical if somewhat expensive. Use of a vector processing computer would significantly reduce the simulation time (by at least an order of magnitude).

REFERENCES

Borgman, L. E., 1969: Ocean wave simulation for engineering design. *J. Waterways Harbors Div., ASCE,* **WW4,** 557–583.

Davenport, W. B., Jr., and W. L. Root, 1958: *An Introduction to the Theory of Random Signals and Noise.* McGraw-Hill.

Eby, E., 1970: Synthesis of multivariate Gaussian random processes with a preassigned covariance. *IEEE Trans. Inform. Theory,* **IT-16,** No. 6.

Hasselmann, K., 1961: On the non-linear energy transfer in a gravity wave spectrum. Part I: General theory. *J. Fluid Mech.,* **12,** 481–500.

—— *et al.,* 1973: Measurement of wind-wave growth and swell decay during the Joint North Sea Wave Project (JONSWAP). *Erganz. Dstch. Hydrogr. Z.* **A8.**

Kennedy, R. M., 1978: A probabilistic description of deep water whitecaps. Ph.D. dissertation, Nova University.

Monahan, E. C., 1971: Ocean whitecaps. *J. Phys. Oceanogr.,* **1,** 139–144.

Pierson, W. J., and L. Moskowitz, 1964: A proposed spectral form for fully developed wind seas based on the similarity theory of S. A. Kitaigorodskii. *J. Geophys. Res.,* **69,** 5181–5190.

Phillips, O. M., and M. L. Banner, 1974: Wave breaking in the presence of wind drift and swell. *J. Fluid Mech.,* **66,** 625–640.

Regier, L. A., and R. E. Davis, 1977: Observations of the power and directional spectrum of ocean surface waves. *J. Mar. Res.,* **35,** 433–451.

Shreider, Y. A., 1966: *The Monte Carlo Method.* Pergamon Press.

Thompson, R., 1973: *Generation of Stochastic Processes With A Given Spectrum.* Utilitas Mathematica, Vol. 3, 127–137.